Global Variability of the Wavenumber Spectrum of Oceanic Mesoscale Turbulence

YONGSHENG XU AND LEE-LUENG FU

Jet Propulsion Laboratory, California Institute of Technology, Pasadena, California

(Manuscript received 19 August 2010, in final form 11 November 2010)

ABSTRACT

The wavenumber spectra of sea surface height from satellite altimeter observations have revealed complex spatial variability that cannot be explained by a universal theory of mesoscale turbulence. Near the edge of the core regions of high eddy energy, agreement is observed with the prediction of the surface quasigeostrophic (SQG) turbulence theory, which has fundamental differences from that of the traditional quasigeostrophic (QG) turbulence theory. In the core regions of high eddy energy, the spectra are consistent with frontogenesis that is not fully accounted for by the SQG theory. However, the observations in the vast ocean interior of low eddy energy exhibit substantial differences from the predictions of existing theories of oceanic mesoscale turbulence. The spectra in these regions may reflect the ocean's response to short-scale atmospheric forcing and air–sea interaction. The observations presented in this paper serve as a test bed for new theories and ocean general circulation models.

1. Introduction

Energy balance in ocean dynamics holds the key to predicting the state of ocean circulation and its evolution. Wind inputs energy to the oceanic general circulation at the ocean basin scales. The energy is then transferred to the mesoscale, roughly defined as wavelengths from 10 to 300 km (note that the length scale is sometimes referred to wavelength divided by 2π), through the instability of ocean currents. The rate and direction of energy cascade in the mesoscale turbulent motions is important to understanding how the energy of ocean circulation is eventually dissipated, a process yet to be fully understood. The distribution of the kinetic energy in the ocean over a range of spatial scales, as expressed by its wavenumber spectrum, provides information on the underlying processes of oceanic mesoscale turbulence. In the wavenumber spectrum, mesoscale turbulence corresponds to the wavenumber band in which the spectral slope is steepest and nearly constant, exhibiting an inertial range, whereas mesoscale eddies correspond to the energy-containing band at lower wavenumbers where the spectral slope levels off (see Fig. 1). There are various theories predicting the shape of the wavenumber spectrum. The observation of sea surface height (SSH) from satellite altimetry presented in the paper makes it possible to examine the validity and generality of the various theoretical predictions on a global scale.

The cascade of oceanic mesoscale energy is accomplished by highly nonlinear turbulent fluid motion. Because this turbulent motion is under a quasigeostrophic balance, it is called quasigeostrophic (QG) turbulence (Charney 1971; Hua and Haidvogel 1986; McWilliams 1989). In the absence of forcing and boundary effects in the interior of the ocean and atmosphere, some interesting properties of QG turbulence have long been derived by Charney (1971) based on the conservation of energy and potential vorticity. The theory of Charney predicts that the energy in the interior of the ocean and atmosphere should cascade from small toward large scales, the so-called inverse cascade. It also predicts a k^{-3} power law for the kinetic energy spectrum, where k denotes wavenumber. Under the geostrophic balance, the wavenumber spectrum of SSH should then follow a k^{-5} power law.

The first opportunity to test this spectral characteristic was the availability of the *Seasat* altimeter data (Fu 1983). In high mesoscale energy regions, the *Seasat* SSH spectrum exhibited a slope close to the k^{-5} power law, whereas in low mesoscale energy regions the spectrum showed k^{-1} dependence. These results were later considered unreliable because of the short duration of the

Corresponding author address: Yongsheng Xu, Jet Propulsion Laboratory, California Institute of Technology, 4800 Oak Grove Drive, Pasadena, CA 91109.
E-mail: yongsheng.xu@jpl.nasa.gov

DOI: 10.1175/2010JPO4558.1

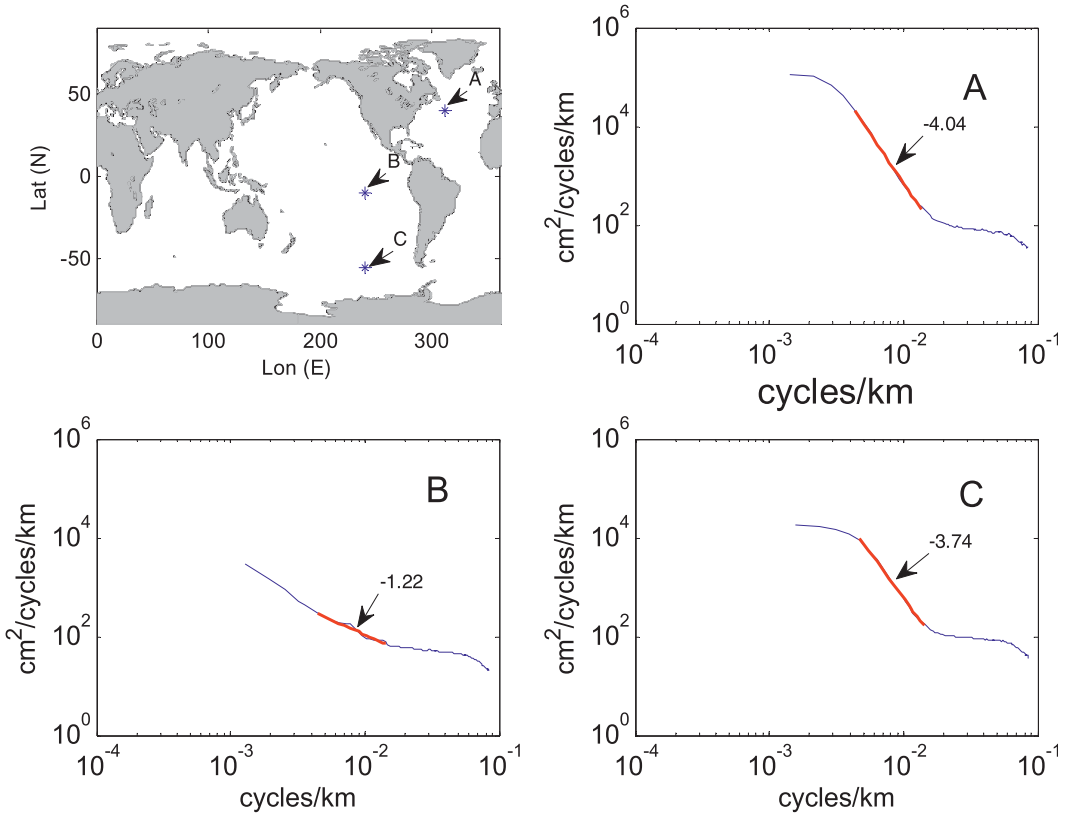

FIG. 1. Selected wavenumber spectra from *Jason-1* observations. (top left) The map shows the locations of the centers (A, B, and C) of 10° × 10° boxes for the averaged wavenumber spectra indicated in the other panels. The red line in the wavenumber spectrum is the fitted slope line in the range between 70 and 250 km, the mesoscale turbulence band. The value of the wavenumber spectrum slope is noted in the plot.

Seasat data. Similar analyses based on longer datasets from later altimeter missions revealed a range of results. Results from the *Geosat* data showed that the spectrum in high energy regions was closer to k^{-4} than k^{-5} and that, in low energy regions, the spectral slopes varied between -2 and -3 (Le Traon et al. 1990). Analysis based on 3 yr worth of the Ocean Topography Experiment (TOPEX)/Poseidon data suggested the existence at midlatitudes of a normalized universal wavenumber spectrum following $k^{-4.6}$ (Stammer 1997). More recent results based on data from multiple satellites, however, called for a $k^{-11/3}$ spectrum in high energy regions (Le Traon et al. 2008).

Given the different results from regional studies noted above, we feel compelled to conduct a systematic global survey of the SSH wavenumber spectrum to evaluate the geographic pattern of spectral slope and its consistency with existing theories. In this paper, we present results from analyzing 7-yr SSH observations made by the *Jason-1* satellite (Ménard et al. 2003), which carries a state-of-the-art radar altimeter system. We have constructed the first global map showing the variability of SSH spectrum. The results are compared to theoretical predictions. The comparison has shed light on the limitations of the existing theories and provided guidance for future studies.

2. Global survey of altimeter wavenumber spectra

We used the *Jason-1* along-track SSH observations over 7 yr from January 2002 to January 2009, covering 259 10-day repeat cycles, to study the SSH wavenumber spectrum. The time mean at each location of observation was first removed to obtain SSH anomalies for spectral computations. The SSH anomaly spectral slopes were then computed via a least squares fit of a power law between 70- and 250-km wavelengths at 2° × 2° grid resolution over the global ocean. The spectrum at each grid point was obtained by averaging all the spectra of SSH anomalies along the *Jason-1* ground tracks that are longer than 500 km within a 10° × 10° box centered at the grid point.

The areas poleward of 60°S and 60°N are excluded from the study to avoid the ice influence on the SSH

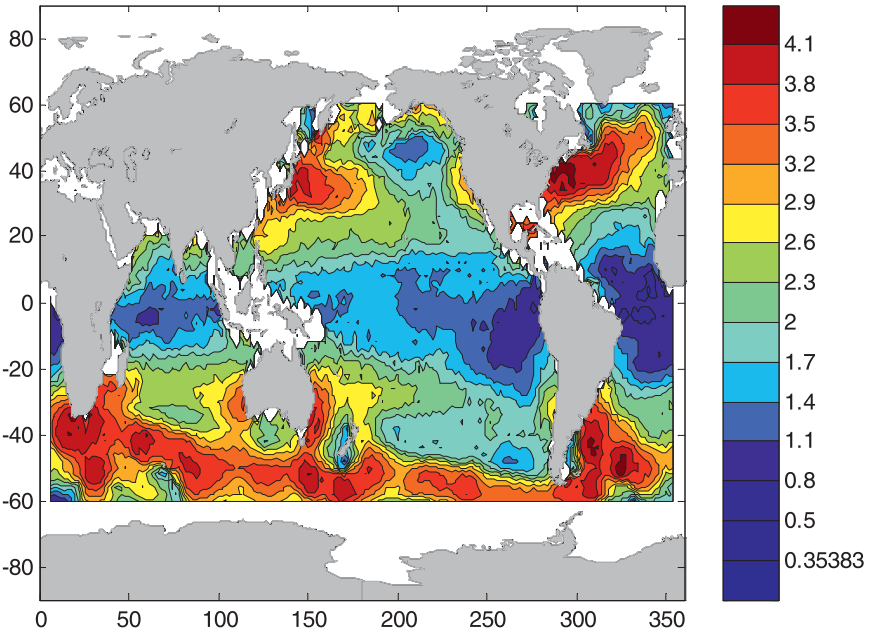

FIG. 2. The global distribution of the spectral slopes of SSH wavenumber spectrum in the wavelength band of 70–250 km estimated from the *Jason-1* altimeter measurements. The sign of the slopes was reversed to make the value positive.

measurements. The wavelength range for computing the spectral slope was selected after a global evaluation of the wavelengths where the SSH spectrum followed a power law: 250 km represents an upper limit beyond which the spectrum levels off to an energy-containing band (except for the tropics, where the energy-containing band is at longer wavelengths); 70 km represents a lower limit, below which the spectrum is dominated by measurement noise. After extensive testing, we found that the results presented in the paper were not sensitive to the choice of the selected wavenumber band to the extent of the estimation error (see appendix).

The wavenumber spectra in a few typical high or lower energy regions are shown in Fig. 1. Note that at midlatitudes the wavelength range of 70–250 km represents a well-defined power-law regime associated with the mesoscale turbulence. In the tropics, however, the spectrum at wavelengths longer than 250 km continues rising, indicating the energy-containing wavelengths are longer than 500 km. Note that the small wiggles in the tropical spectrum are caused by the tropical instability waves (Willett et al. 2006). Because the *Jason-1* orbit has an inclination of 66°, its ground tracks sample primarily the meridional variability in the tropics. The meridional scales of the tropical instability waves on the order of 200 km are reflected by the small wiggles in the spectrum.

Figure 2 displays a map showing the geographic variability of the SSH wavenumber spectral slope of the global oceans. The result is quite surprising: the steepest spectral slope of the global ocean is -4.2 ± 0.11 (see appendix for error estimation), which is significantly flatter than the k^{-5} power law predicted by the QG theory. For the vast extratropical oceans that had been suggested as a geostrophically turbulent ocean (Stammer 1997), the slopes have a wide range, from -4.2 to -0.7. The major current systems, where the dynamics are highly nonlinear, have steeper slopes than other areas. Note that, even in the most typical high-energy regions (e.g., the Gulf Stream), the steepest slope (i.e., -4.2) is still quite different from the k^{-5} power law. This result presents clear evidence that the observed SSH spectral slopes are significantly flatter than the prediction of the QG turbulence theory everywhere in the ocean.

The recent results of Le Traon et al. (2008) showing a $k^{-11/3}$ power law at high eddy-energy regions are consistent with Fig. 2 in many regions near the major extratropical current systems where strong eddies are generated, such as the Gulf Stream, the Kuroshio, the Agulhas Current, and the Antarctic Circumpolar Current. The $k^{-11/3}$ power law for the SSH spectrum is consistent with the theory of surface quasigeostrophic (SQG) turbulence. The SQG theory considers the effects of boundaries in the ocean and atmosphere (Blumen 1978; Held et al. 1995). Driven by density perturbations on the ocean surface, the kinetic energy spectrum in the upper ocean should exhibit a $k^{-5/3}$ power law, leading to $k^{-11/3}$ for the SSH spectrum.

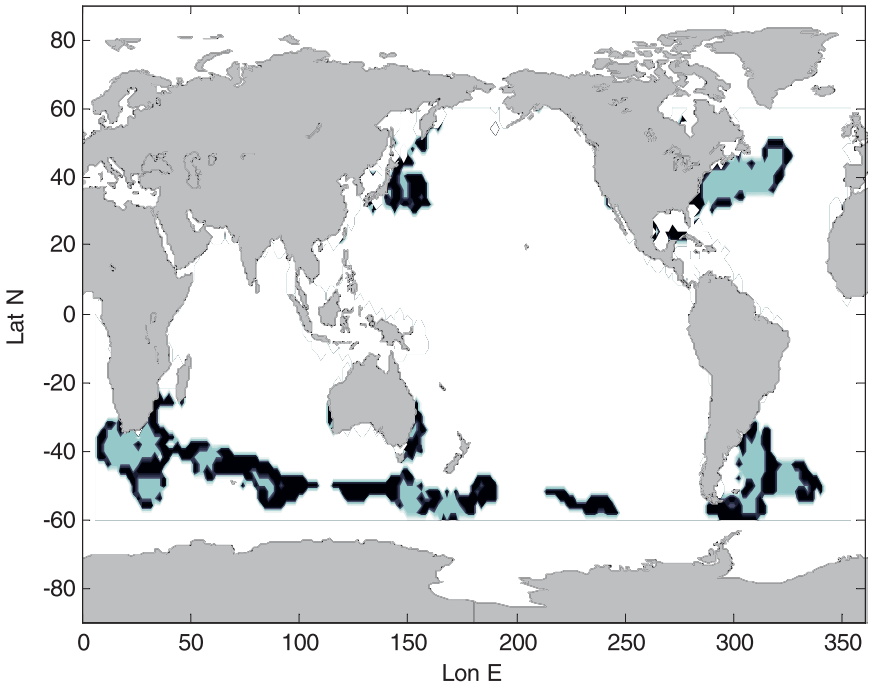

FIG. 3. Three types of areas in terms of the spectral power law. The black color represents the type-1 areas where the spectral slopes follow the SQG $k^{-11/3}$ power law within the 95% confidence level, the gray color represents the type-2 areas where the spectral slopes are steeper than $k^{-11/3}$, and the white color represents the type-3 areas where the spectral slopes are flatter than $k^{-11/3}$.

In addition to spectral slopes, the SQG turbulence theory also predicts an inverse cascade of surface kinetic energy (Capet et al. 2008a) from small to large scales. This prediction was validated by the results of Scott and Wang (2005), who computed energy flux in wavenumber spectral space from satellite altimeter data and demonstrated an inverse cascade of baroclinic energy from scales of the Rossby radius of deformation to larger scales. However, these results are in contradiction to the prediction of the classical QG turbulence theory. The QG theory predicts a cascade of baroclinic energy from both large and small scales toward the Rossby radius of deformation, where the energy is converted into the barotropic mode and then an inverse cascade takes place, transferring barotropic energy from the Rossby radius of deformation toward larger scales (Salmon 1980; Smith and Vallis 2001; Fu and Flierl 1980).

To examine the applicability of the SQG-predicted $k^{-11/3}$ power law in the ocean, Fig. 3 exhibits the areas in which the SSH spectral slopes are indistinguishable from $-11/3$ within the 95% confidence level. We categorize the global ocean into three types of regions. The type-1 regions, denoted by black color, are where the SQG theory applies. They are quite patchy and most of them tend to form around the regions of the highest eddy energy (e.g., the Gulf Stream, the Brazil–Malvinas Confluence, and the Agulhas Current). In such cases, they are in the transition zones from the edge to the core of the major current systems. The type-2 regions, denoted by gray color, are where the spectral slopes are significantly steeper than $k^{-11/3}$. They include the core regions of the current systems mentioned above. The spectral slopes in these regions are close to k^{-4}, consistent with a k^{-2} kinetic energy spectrum of an ocean dominated by the presence of fronts (Boyd 1992). In fact, the inverse cascade of kinetic energy predicted by the SQG theory dictates an energy flux from frontogenesis to convert potential energy to kinetic energy (Capet et al. 2008a). This implies the incompleteness of the SQG theory, which does not include frontogenesis. The transition of near k^{-4} SSH spectrum to $k^{-11/3}$ spectrum in the high eddy-energy regions requires more theoretical work to explain.

The type-3 regions, denoted by white color, include the tropical oceans and the vast extratropical areas outside major current systems. In this vast majority of the global ocean, the SSH spectral slopes are significantly flatter than $k^{-11/3}$. This has raised concerns for the effects of measurement errors, which may cause the flatness of the SSH spectrum in the low energy regions.

As noted earlier, the instrument noise is responsible for a near-white spectral level that limits the analysis to wavelengths longer than 70 km. As shown in Fig. 4, other sources of errors from ocean waves and atmospheric media effects have much less variance than the SSH spectral level at wavelengths of 70–250 km, suggesting that the spectra in the type-3 regions are most likely associated with oceanic signals.

3. Discussion

The findings presented in Figs. 2–3 have posed a question on our understanding of the dynamics governing the upper-ocean turbulence in the wavelength regime of 70–250 km. It is apparent that nowhere in the ocean is the observed SSH wavenumber spectrum consistent with the classical QG turbulence theory. This is not surprising because the QG theory is not intended to be applicable to the upper ocean, although there have been considerable efforts in the past trying to use the theory to interpret the upper-ocean observations. In particular, Stammer (1997) suggested that, after the application of an ad hoc error correction to altimeter data, the resulting spectrum was close to k^{-5}, as predicted by the QG turbulence theory. However, we felt that such a correction was not justified in light of Fig. 4, which shows that the magnitudes of measurement errors other than instrument noise are much less than that of ocean signals. Without the error correction, Stammer (1997) would not have obtained a universal spectrum with a slope close to -5.

The realization of the efficacy of the SQG theory in explaining the upper-ocean SSH spectrum in certain high energy regions (Le Traon et al. 2008) was encouraging. Le Traon et al. (2008) investigated only the high energy regions: the Gulf Stream, the Kuroshio, and the Agulhas Current regions. They found that the spectral slopes in these regions were between -3.4 and -3.7 with a mean value of -3.6, which are basically in agreement with our results in these three regions. The slight difference might be caused by the difference in the size of the domain box analyzed. Their box size was twice as large as our box size in longitudes. However, our findings have shown that the applicability of the SQG theory is limited to regions primarily in the transition zones from the edge to the core of the high energy regions of the major ocean current systems. In the core regions of high eddy energy, the spectrum is close to k^{-4} and consistent with the dominance of fronts that cannot be fully accounted for by the SQG theory (Boyd 1992). There is a need for a new theory to explain the details of the spectral slopes from $k^{-11/3}$ to k^{-4} in these regions. On the other hand, one might argue that the distinction between $k^{-11/3}$ and k^{ι} is not attainable with statistical confidence and thus conclude that the SSH spectrum in these regions is not inconsistent with the framework of the SQG theory and the presence of fronts.

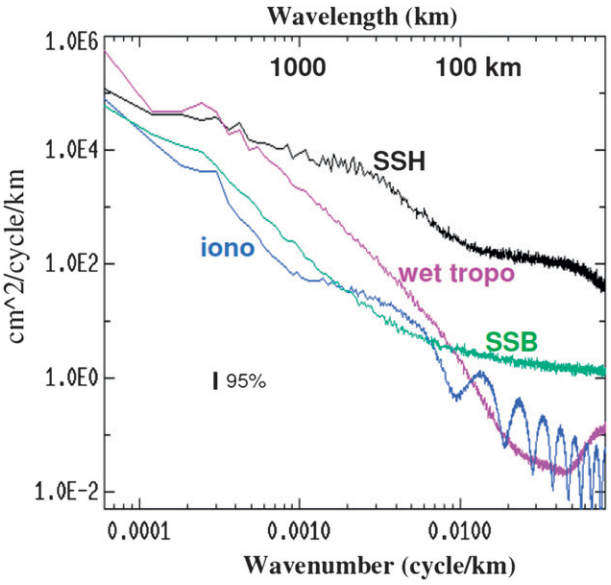

FIG. 4. SSH spectrum (black) from *Jason-1* altimeter observations in the low eddy-energy regions of the eastern Pacific Ocean. Superimposed are the spectra of various corrections for the long-wavelength errors in the altimeter data: wet tropospheric correction (cyan), sea-state bias (SSB; green), and ionospheric correction (blue). Note that the spectral levels of these corrections are lower than that of SSH by more than one order of magnitude in the wavelength range of 70–250 km. The residual errors after the application of these corrections are even smaller. This figure illustrates that the spectral estimates presented in the paper are not affected by long-wavelength errors (the apparent oscillations in the ionosphere correction are caused by boxcar smoothing over 100 km).

Another plausible interpretation might be that the type-1 regions are just transitions in which there is a blend of variability with type-2 spectral rolloff and type-3 spectral rolloff, thus resulting in an intermediate spectral rolloff not necessarily attributable to the SQG theory. However, we believe that the SQG theory does play an important role in these regions. Otherwise, it is hard to explain the close relationship between SSH and sea surface temperature (SST) revealed by observations in the Gulf Stream region at scales between 80 and 300 km (Isern-Fontanet et al. 2006) and the inverse cascade observed by Scott and Wang (2005), as predicted by the SQG theory.

The dynamics of the type-3 regions are in a more linear regime than that of the strong current systems. Because of their low energy levels, the effects of Rossby wave dispersion tend to dominate those of nonlinear advection. The degree of linearity can be evaluated by the so-called Rhines parameter $U/(\beta L^2)$, where U is a velocity scale, L is a length scale, and β is the

meridional derivative of the Coriolis parameter (Rhines 1979). Chelton et al. (2010) presented a global map of this parameter, which is generally less than unity in the type-3 regions, consistent with linear dynamics. Frankignoul and Müller (1979) studied the ocean's linear response to stochastic wind forcing, suggesting k^{-1} to k^{-2} wavenumber spectrum for the energy of the ocean's response at scales shorter than the baroclinic radius of deformation at midlatitudes. This implies k^{-3} to k^{-4} SSH spectrum, steeper than the altimetry spectrum in the type-3 regions. However, the forcing used by Frankignoul and Müller (1979) may not be adequate at high wavenumbers and thus could not result in correct prediction of the ocean's response.

The overall pattern of the spatial variability of the wavenumber spectral slope depicted in Fig. 2 is quite similar to the pattern of global distribution of eddy variability. In general, the higher is the eddy variability, and the steeper is the spectral slope. This is roughly in line with the argument that the steep spectrum is associated with highly nonlinear dynamics and the flat spectrum is associated with more linear dynamics. To show this relationship graphically, Fig. 5 displays scatter diagrams of the variance of SSH variability versus the slope of the wavenumber spectral slope. The SSH variance was computed from the gridded altimetry data from 1993 to 2009 produced by Archiving, Validation, and Interpretation of Satellite Oceanographic data (AVISO) based on the procedures described in Ducet et al. (2000). At latitudes higher than 25°, there is a fairly tight linear relationship between the SSH variance (in logarithm scale) and the spectral slope. If the low latitude regions are also included, the relationship becomes a bit fuzzier. This is caused by the distinction of the tropical dynamics from the midlatitude dynamics.

High-resolution numerical model simulations have been analyzed for wavenumber spectral slopes in some regions of energetic ocean currents (Capet et al. 2008b; Klein et al. 2008). These results show that the slope of kinetic energy spectrum is close to k^{-2}, consistent with the k^{-4} SSH spectrum of the present study. It will be interesting to conduct a similar survey of the global variability of spectral slope from the state-of-the-art ocean general circulation models. In particular, the models should be forced by realistic fluxes of momentum and heat, especially at high wavenumbers to explore the spectral properties in the type-3 regions. The results from the present study will serve as a test bed for the model simulations.

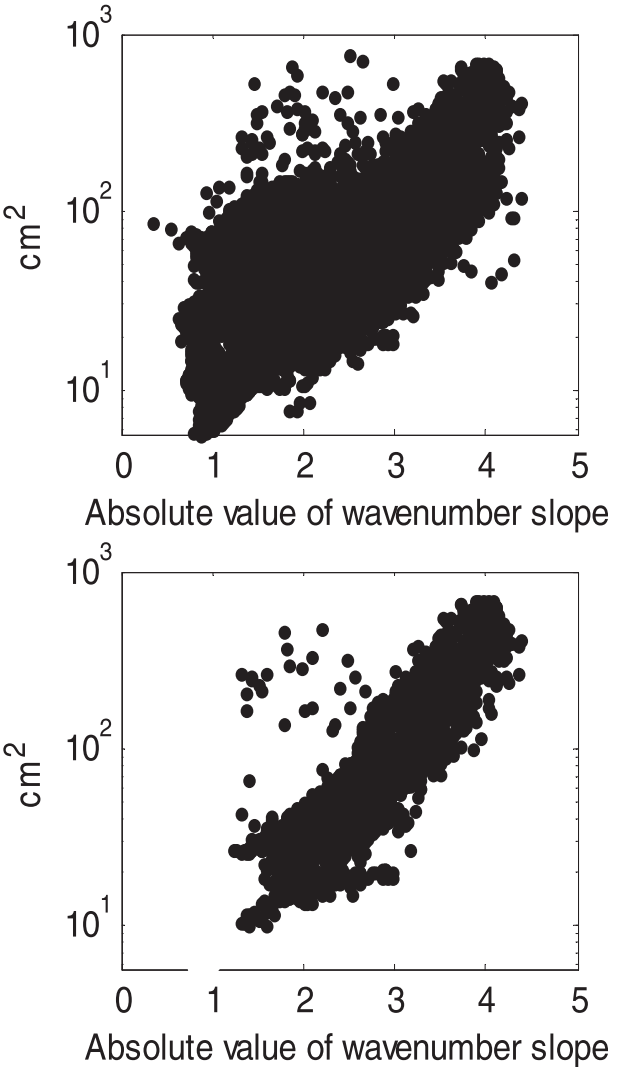

FIG. 5. Scatter diagram between the SSH variance estimated from the AVISO data and the wavenumber spectral slope in the wavelength band of 70–250 km estimated from the *Jason-1* altimeter measurements. Note that we have conducted the same 10° × 10° box smoothing for the SSH variance as for the wavenumber spectrum. (top) For all regions and (bottom) for regions within midlatitude ranges (25°–45°N) and (25°–45°S).

Acknowledgments. The research presented in the paper was carried out at the Jet Propulsion Laboratory, California Institute of Technology, under contract with the National Aeronautics and Space Administration. Support from the *Jason-1* and OSTM/Jason-2 projects is acknowledged. The authors thank Raffaele Ferrari, James McWilliams, Dudley Chelton, and Patrice Klein for their comments.

APPENDIX

Estimate of the Wavenumber Spectral Slope Error

A spectral slope error was estimated for each pass within the 10° × 10° box centered at a given grid point.

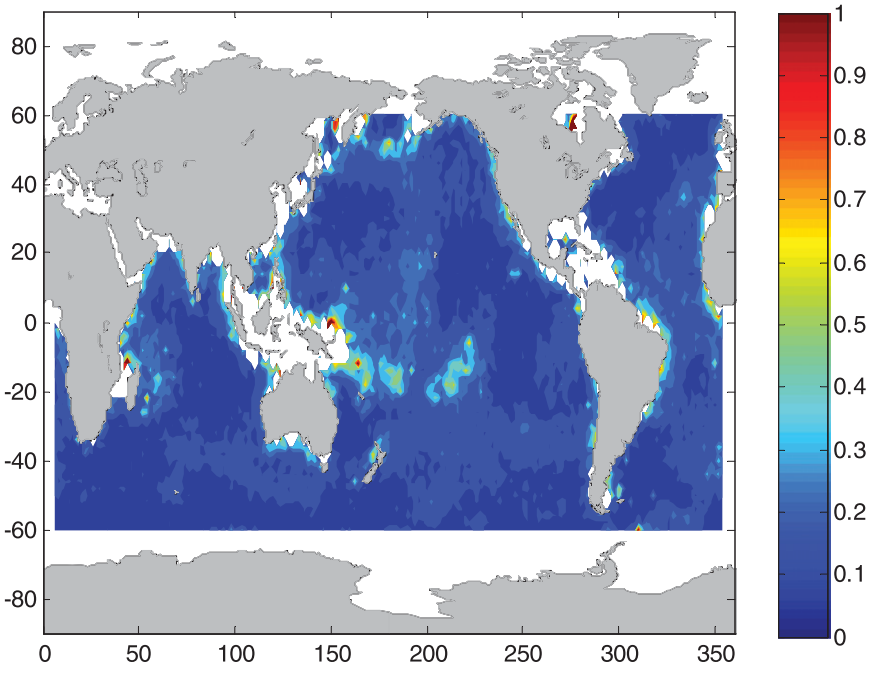

FIG. A1. The error bar at 95% confidence level of the spectral slopes of SSH wavenumber spectrum in the wavelength band of 70–250 km estimated from the *Jason-1* altimeter measurements.

Then the slope error at the grid point was obtained as $\sum_1^m e_i^2/m$, where m is the total number of passes in the $10° \times 10°$ box and e_i is the slope error of the ith pass. For each pass, an averaged spectrum was computed from the spectra of all the repeat along-track measurements (one per cycle). Only those cycles with good data exceeding 95% were included in the analysis.

The remaining small gaps were filled by linear interpolations. The relatively few interpolations did not have any significant smoothing effects on the spectrum.

A linear equation was fitted to each averaged spectrum using a least squares method as follows:

$$y = \beta_0 + \beta_1 x, \tag{A1}$$

where $y = \log_{10}P$ and $x = \log_{10}k$; P is the spectral power at wavenumber k. The confidence interval of the slope regression coefficient β_1 is given by the equation (Montgomery et al. 2001)

$$e = t_{\alpha/2,n-2} \cdot \sqrt{\frac{\sum_{j=1}^{n} (\Delta y_j)^2}{\sum_{j=1}^{n} (x_j - \overline{x})^2}}, \tag{A2}$$

where $t_{\alpha/2,n-2}$ is the percentile of the t distribution with α level of significance and $(n - 2)$ degrees of freedom, which is the number of the data. In our case, n is given by the number of data points in the wavenumber range [1/250 km, 1/70 km], typically about 10. The square root term is the standard error of the estimate of the slope regression coefficient β_1. In our case, $\alpha = 0.05$ and Δy represents the difference between the fitted and real value of y. The calculated error bar for the global ocean is shown in Fig. A1.

REFERENCES

Blumen, W., 1978: Uniform potential vorticity flow: Part I. Theory of wave interactions and two-dimensional turbulence. *J. Atmos. Sci.,* **35,** 774–783.

Boyd, J. P., 1992: The energy spectrum of fronts: Time evolution of shocks in Burger's equation. *J. Atmos. Sci.,* **49,** 128–139.

Capet, X., P. Klein, B. Hua, G. Lapeyre, and J. C. McWilliams, 2008a: Surface kinetic energy transfer in surface quasi-geostrophic flows. *J. Fluid Mech.,* **604,** 165–174.

——, J. C. McWilliams, M. J. Molemaker, and A. F. Shchepetkin, 2008b: Mesoscale to submesoscale transition in the California Current System. Part I: Flow structure, eddy flux, and observational tests. *J. Phys. Oceanogr.,* **38,** 29–43.

Charney, J. G., 1971: Geostrophic turbulence. *J. Atmos. Sci.,* **28,** 1087–1094.

Chelton, D. B., M. G. Schlax, and R. M. Samelson, 2011: Global observations of nonlinear mesoscale eddies. *Prog. Oceanogr.,* doi:10.1016/j.pocean.2011.01.002, in press.

Ducet, N., P. Y. Le Traon, and G. Reverdin, 2000: Global high resolution mapping of ocean circulation from the combination of TOPEX/POSEIDON and ERS-1/2. *J. Geophys. Res.,* **105,** 19 477–19 498.

Frankignoul, C., and P. Müller, 1979: Quasi-geostrophic response of an infinite β-plane ocean to stochastic forcing by the atmosphere. *J. Phys. Oceanogr.,* **9,** 104–127.

Fu, L.-L., 1983: On the wave number spectrum of oceanic mesoscale variability observed by the SEASAT altimeter. *J. Geophys. Res.,* **88,** 4331–4341.

——, and G. R. Flierl, 1980: Nonlinear energy and enstrophy transfers in a realistically stratified ocean. *Dyn. Atmos. Oceans,* **4,** 219–246.

Held, I. M., R. T. Pierrehumbert, S. T. Garner, and K. L. Swanson, 1995: Surface quasi-geostrophic dynamics. *J. Fluid Mech.,* **282,** 1–20.

Hua, B. L., and D. B. Haidvogel, 1986: Numerical simulations of the vertical structure of quasi-geostrophic turbulence. *J. Atmos. Sci.,* **43,** 2923–2936.

Isern-Fontanet, J., B. Chapron, G. Lapeyre, and P. Klein, 2006: Potential use of microwave sea surface temperatures for the estimation of ocean currents. *Geophys. Res. Lett.,* **33,** L24608, doi:10.1029/2006GL027801.

Klein, P., B. L. Hua, G. Lapeyre, X. Capet, S. Le Gentl, and H. Sasaki, 2008: Upper ocean turbulence from high-resolution 3D simulations. *J. Phys. Oceanogr.,* **38,** 1748–1763.

Le Traon, P. Y., M. C. Rouquet, and C. Boissier, 1990: Spatial scales of mesoscale variability in the North Atlantic as deduced from Geosat data. *J. Geophys. Res.,* **95,** 20 267–20 285.

——, P. Klein, and B. L. Hua, 2008: Do altimeter wavenumber spectra agree with the interior or surface quasigeostrophic theory? *J. Phys. Oceanogr.,* **38,** 1137.

McWilliams, J. C., 1989: Statistical properties of decaying geostrophic turbulence. *J. Fluid Mech.,* **108,** 199–230.

Ménard, Y., and Coauthors, 2003: Jason-1 calibration/validation. *Mar. Geod.,* **26,** 131–146.

Montgomery, D. C., E. A. Peck, and G. G. Vining, 2001: *Introduction to Linear Regression Analysis*. 3rd ed. Wiley, 641 pp.

Rhines, P. B., 1979: Geostrophic turbulence. *Annu. Rev. Fluid Mech.,* **11,** 401–441.

Salmon, R. S., 1980: Baroclinic instability and geostrophic turbulence. *Geophys. Astrophys. Fluid Dyn.,* **15,** 167–221.

Scott, R. B., and F.-M. Wang, 2005: Direct evidence of an oceanic inverse kinetic energy cascade from satellite altimetry. *J. Phys. Oceanogr.,* **35,** 1650–1666.

Smith, K. S., and G. K. Vallis, 2001: The scales and equilibration of midocean eddies: Freely evolving flow. *J. Phys. Oceanogr.,* **31,** 554–571.

Stammer, D., 1997: Global characteristics of ocean variability estimated from regional TOPEX/Poseidon altimeter measurements. *J. Phys. Oceanogr.,* **27,** 1743–1769.

Willett, C. S., R. Leben, and M. F. Lavın, 2006: Eddies and mesoscale processes in the eastern tropical Pacific: A review. *Prog. Oceanogr.,* **69,** 218–238.